JOURNAL OF SPACECRAFT AND ROCKETS
Vol. 31, No. 2, March–April 1994

Investigation of the Flow past the ARIANE 5 Launcher Afterbody

Philippe Reijasse* and Jean Délery†
Office National d'Etudes et de Recherches Aérospatiales, 92320 Châtillon, France

The flow past a 0.01-scale model of the ARIANE 5 European launcher afterbody was investigated in detail to establish a clear picture of the flowfield structure in the base region of the launcher. The experimental setup consisted of a Mach 4 contoured annular nozzle equipped with a centerbody-mounted model. The model itself reproduced the central engine and the two lateral boosters of the launcher first stage. The propulsive nozzles were supplied by cold high-pressure air with expansion ratios simulating a flight altitude close to 30 km. The flow around the afterbody was defined using surface pressure measurements, visualization techniques (surface flow pattern, schlieren photographs), and a three-component laser velocimeter system. These experimental results will help in the physical understanding of complex flows and in providing well-documented test cases to validate three-dimensional Navier-Stokes calculations.

I. Introduction

DURING the ascent of a multinozzle launcher, its afterbody is subjected to high heat transfer rates. This fact was clearly observed in the first stage base region of the TITAN 3C,[1] the arrangement of which is similar to that chosen for the future ARIANE 5 launcher. Both radiative and convective heat transfer were measured at two locations of a TITAN base (see Fig. 1). The results obtained clearly show that the radiative component is preponderant during the first seconds but rapidly decreases with flight altitude while the convective flux increases sharply to become the main component. Similar behavior was observed on the Space Shuttle.[2]

The nature of convective phenomena around a multinozzle afterbody mainly results from the conjunction of two parameters: the flight altitude (in other words—nozzle expansion ratio) and the powerplant configuration (number of nozzles, confined space between them, their clustered disposition, etc.).[3] In particular, for a four-nozzle afterbody, several experimental studies[4–7] showed that two kinds of afterbody flow regimes exist.

At low altitude, the entrainment effect of the overexpanded or near-adaptation propulsive jets ensures the evacuation from the base region of a mass flux issued from the cold external flow. This flow regime, called the *aspiration regime,* is characterized by weak or even negative convective fluxes.

At high altitude, if the jet pluming effect is strong enough to induce an external flow separation, hot gases recirculating inside the separated zone can impact the aftpart of the launcher fuselage. This *backflow regime* generates high heat transfer rates, possibly increased by a recombustion—or postburning—of incompletely burned species issued from the jets. Under these conditions, it can be seen that the thermal environment at a launcher base strongly depends on the aerodynamic regime in this region.

Briefly speaking, base flow aerodynamics is treated by two kinds of calculation methods. The first one, often called multicomponent-type approach, has led to the development of codes that have demonstrated their validity in numerous two-dimensional or axisymmetric configurations.[8–10] For a three-dimensional afterbody, like the one considered in the present study, the only reliable theoretical approach is to solve the full-time-averaged Navier-Stokes equations.[11–13] However, advanced Navier-Stokes methods still need well-documented experimental data to firmly assess their validity in terms of numerical accuracy and of realistic modeling of turbulence.

Consequently, a detailed experimental analysis of the flowfield around the afterbody of the future ARIANE 5 multinozzle

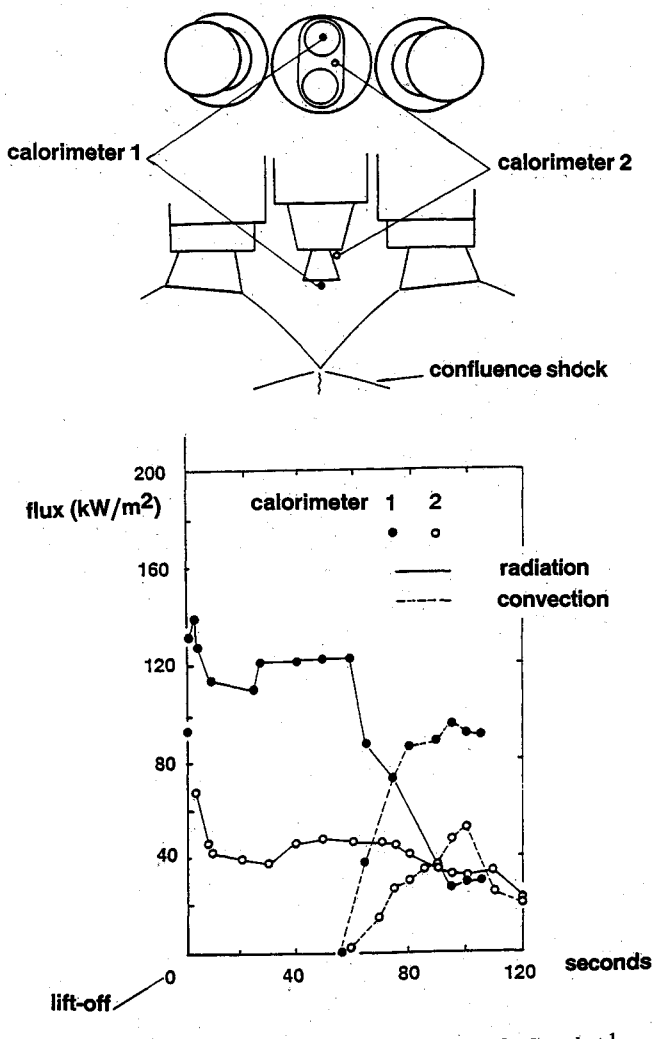

Fig. 1 Heat transfer rates at the base of a TITAN-3C rocket.[1]

Presented as Paper 91-2897 at the AIAA Atmospheric Flight Mechanics Conference, New Orleans, LA, Aug. 12–14, 1991; received Oct. 26, 1991; revision received June 16, 1992; accepted for publication Sept. 14, 1992.

*Research Group Leader, Fundamental Aerodynamics Branch, Aerodynamics Department.
†Head, Fundamental Aerodynamics Branch, Aerodynamics Department. Member AIAA.

launcher was undertaken: first, to help in the prediction of its thermal environment; and second, to constitute a test case for the validation of Navier-Stokes codes. The aim of this article is to present a summary of this study and its most significant results; more detailed information has been provided elsewhere.[14,15]

II. Test Facility and Model Description

Simulated Flight Conditions and Test Setup

The test arrangement had to simulate the flowfield around the ARIANE 5 launcher afterbody at a 30-km flight altitude. This corresponds to an outer Mach number M_0 close to 4 and nozzle expansion ratios p_j/p_0 in the range of 30–50 for the two lateral booster nozzles and in the range of 10–20 for the central engine nozzle. Small changes in altitude could be simulated by varying the stagnation pressures of the jets. The value of the central-to-lateral jet stagnation pressure ratio was close to 5.

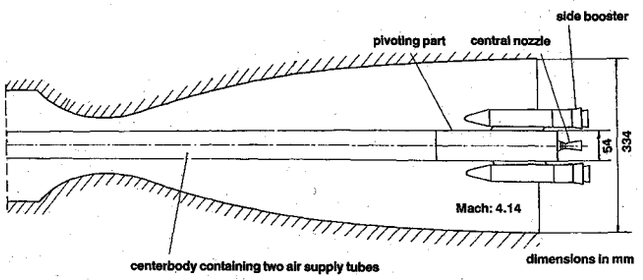

Fig. 2 Arrangement of the contoured nozzle with the centerbody-mounted model.

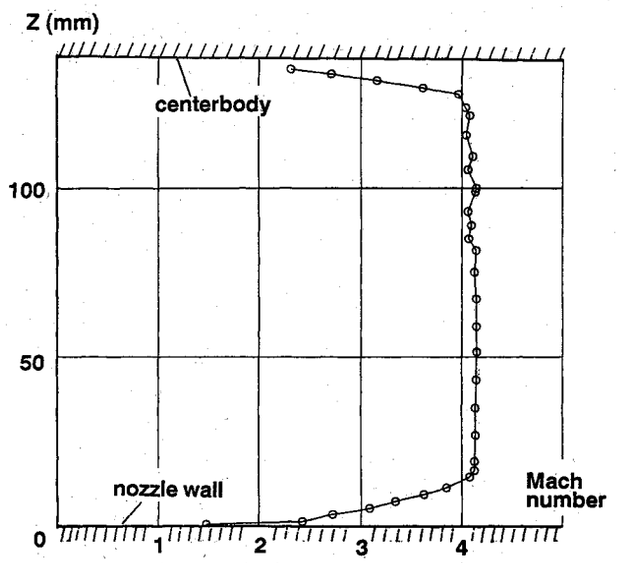

a) Mach number distribution

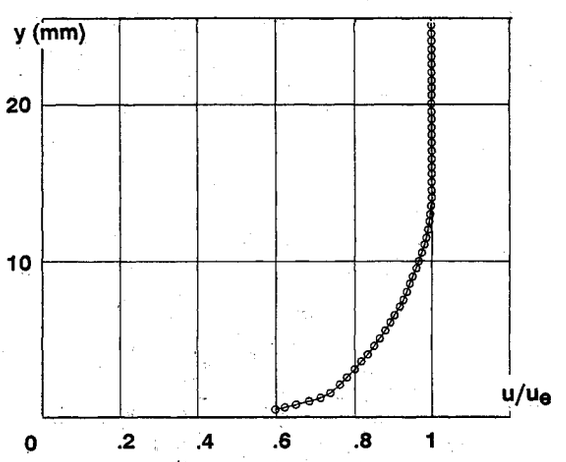

b) Centerbody boundary layer profile

Fig. 3 External flow properties near the nozzle exit section.

These experiments were performed in a blow-down supersonic wind tunnel in the test section of which was mounted an annular nozzle equipped with a centerbody, as shown in Fig. 2. The contour of the nozzle diverging part was computed to obtain a uniform supersonic flow in the test section, taking into account the presence of the center rod. This arrangement is preferable to the use of a lateral strut, which creates strong perturbations in the supersonic stream. The exit diameter of the nozzle is equal to 334 mm and the rod diameter to 54 mm. The wind-tunnel stagnation pressure p_{st0} was set at a value close to 4.10^5 Pa, the stagnation temperature T_{st0} being equal to 410 K. The Mach number distribution, deduced from a Pitot probe survey performed in the nozzle exit section, is shown in Fig. 3a. For this survey, the study model was replaced by a cylindrical extension of the center rod. One sees that, outside the nozzle and rod boundary layers, the flow uniformity is good. The average Mach number in the perfect fluid region is equal to 4.14, with a maximum uncertainty of 0.03. Figure 3b gives the profile of the boundary layer on the center rod measured 6 mm upstream of the nozzle exit section. This profile can be used to determine the upstream boundary conditions of a Navier-Stokes calculation.

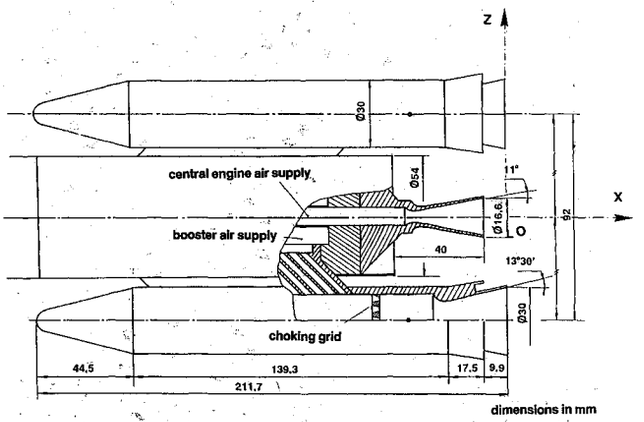

Fig. 4 Afterbody model internal arrangement.

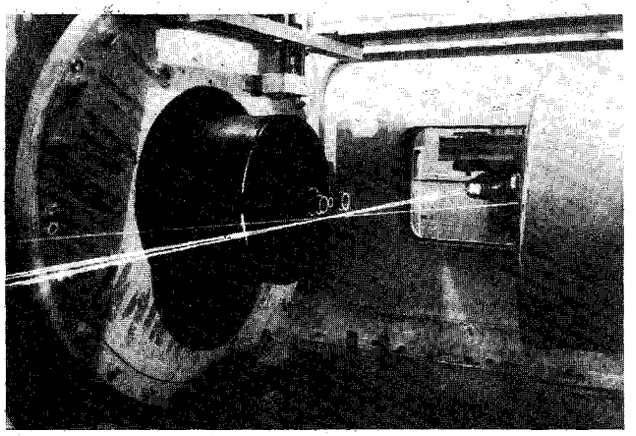

Fig. 5 Model in the test section with LDV system operating.

Model Arrangement

The model arrangement is shown in Fig. 4. The central nozzle and the lateral nozzles are supplied by means of two different concentric tubes. This allows each nozzle expansion ratio to be adjusted independently.

The main features of the model nozzles are also shown in Fig. 4. The real launcher will be equipped with contoured nozzles. However, simpler conical nozzles have been used here due to the small

dimensions of the model. The propulsive jets were simulated using high-pressure air, up to a maximum stagnation pressure of 200.10^5 Pa, at a stagnation temperature close to 400 K. The nozzle diverging angles and area ratios that best reproduced the computed shape of the actual plumes of hot combustion gases were determined by applying a similitude rule.[14] Thus, the nominal Mach numbers of the central nozzle and of the booster nozzles are equal to 4.4 and 2.6, respectively. The sting-mounted afterbody model could be rotated around the sting axis to facilitate Laser Doppler Velocimetry (LDV) measurements. More details concerning the model mounting and the wind-tunnel nozzle are reported elsewhere.[14,15]

III. Means of Investigation

The afterbody was equipped with 35 static pressure holes located on the rear part of the model and inside the nozzles to obtain continuous measurements of the jet stagnation pressure. Pressure measurements will not be presented in this article, attention being focused here on the flowfield structure. Schlieren photographs of the afterbody flow were taken for the different values of the nozzle expansion ratio. Surface flow on the afterbody was visualized by a classical oil-film technique. The resulting surface flow patterns gave precise information for a better understanding of the afterbody flowfield structure.

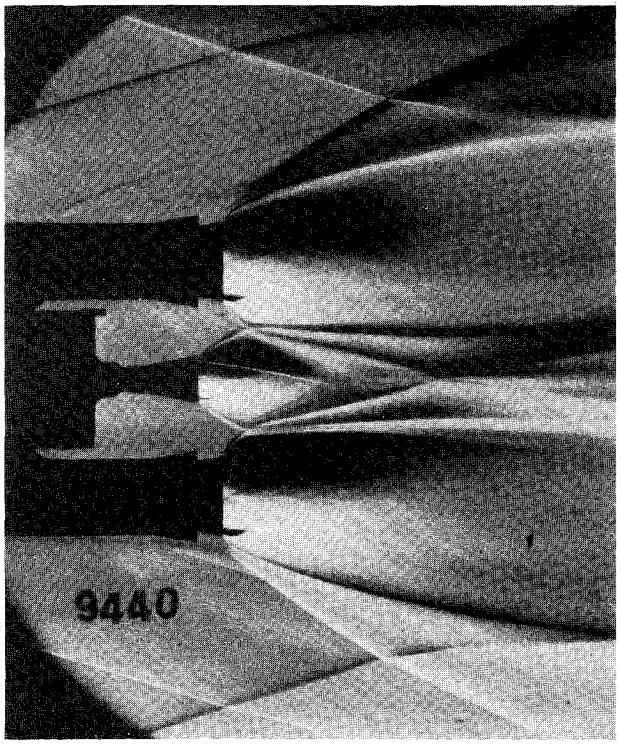

Fig. 6 Schlieren photograph of jets with external flow. Nozzle expansion ratio: central engine $(p_j/p_0)_c = 19.9$ and lateral booster engine $(p_j/p_0)_l = 50.6$.

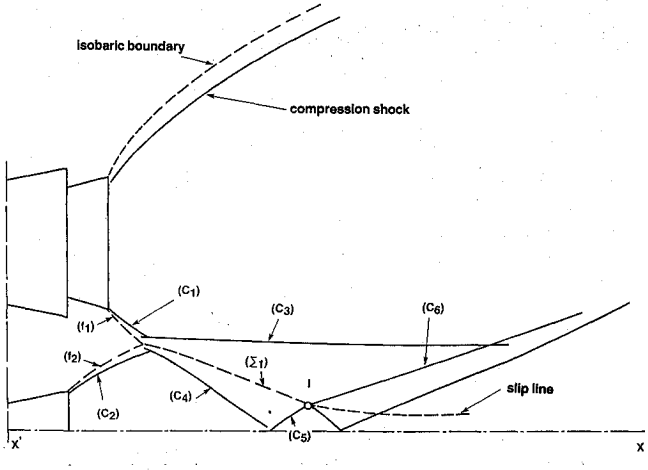

Fig. 7 Interpretation of the shock system resulting from the booster and central engine jet interaction.

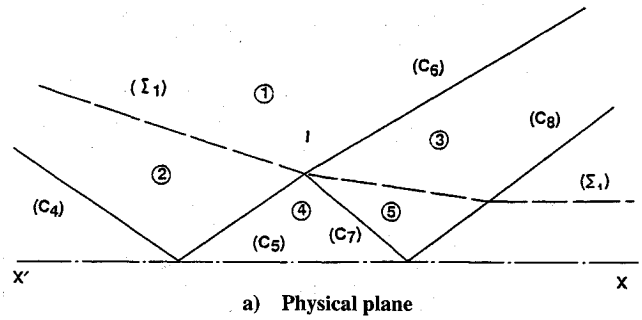

a) Physical plane

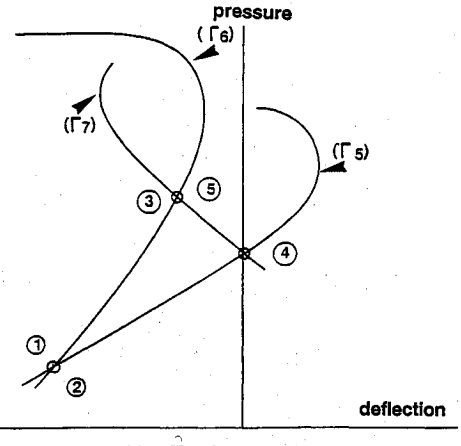

b) Shock polar diagram

Fig. 8 Interpretation of situation at interference point I.

The mean velocity vector field around the afterbody model was investigated using a three-component laser velocimeter.[16] This system is equipped with two 15-W argon lasers. One operating in an all-line mode at a power of 6 W is used for the green (3 W) and blue (3 W) components. The other is used at its maximum power (3 W) on the violet line only. In this way, each fringe pattern receives the same light power.

The three pairs of beams, resulting from traversing of beam splitters, focus to constitute a probe volume with a diameter approximately equal to 400 μm. Interference of the blue and green beams, both contained in a horizontal plane for the present application, produce two fringe patterns contained in a plane normal to the emission line. The violet beam, also in a horizontal plane but in a 25.7-deg direction in comparison with the other emission line, generates a third fringe pattern. Bragg cells are used to determine the direction of each velocity vector component. Because of the very high velocities to be measured, the LDV system was operated in the forward-scattering mode.

At each measurement point, 200 instantaneous values for each velocity component were collected, corresponding to the crossing of the probe volume by 200 particles. The flow was seeded with 0.5-μm-diam latex balls using an injection system located in the wind-tunnel settling chamber, upstream of the nozzle. There was no special seeding of the air feeding the afterbody nozzles.

The relatively small size of the sample collected at each measurement point was dictated by the blow-down operating mode of the facility. However, this size is sufficient to give a statistically acceptable scatter on mean velocity measurements. Measurement accuracy, in the outer unseparated flow, was between 1 and 2%, as concerns mean velocity. In the recirculating regions, the accuracy was close to 10%, because of difficulties met in seeding and probing these zones. The photograph in Fig. 5 shows the test setup installed in the wind-tunnel testing chamber. One sees the exit sec-

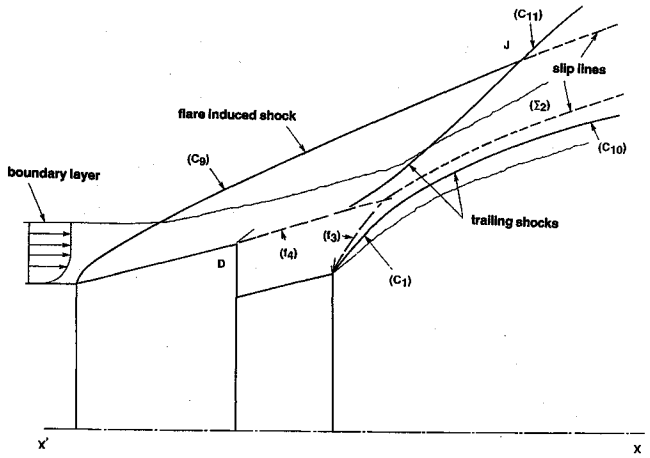

Fig. 9 Interpretation of the flow structure at the booster jet and external flow confluence.

tion of the outer Mach 4 nozzle, the three nozzles of the afterbody and also the three pairs of laser beams emanating from the LDV system emitting part, which is visible in the rear part of the view.

IV. Presentation and Discussion of Results

Flowfield Visualizations

A schlieren photograph of the afterbody flow in jet-on conditions is shown in Fig. 6. The static pressure ratios p_j/p_0 for the central and the lateral jets, indices c and l, respectively, are equal to 19.9 and 50.6. This picture clearly reveals the shock structures generated by the jet/jet and the jet/external stream interactions.

First, let us consider the confluence region between the jets and the corresponding interpretative sketch (Fig. 7), in which we shall note the following:

1) The compression shocks C_1 and C_2 originating very near the nozzle exit and closely following the jet boundaries.

2) The mixing zones developing along the isobaric boundaries f_1 and f_2.

3) The jet confluence region where flow deflections generate shocks C_3 and C_4.

Since shock C_4 is weaker than C_3, a well-marked slip line Σ_1, issuing from the confluence region, separates the booster jet from the central jet. No Mach disk structure appears—shock C_4 reflecting in a regular manner on the symmetry axis. The flow structure in the small region where Σ_1 is near the symmetry axis is difficult to see. A possible interpretation of this phenomenon is sketched in Fig. 8. Interference of the reflected shock C_5 and slip line Σ_1 at point I generates two other shocks, C_6 and C_7, which propagate in the booster jet and in the central nozzle jet, respectively. The reflection of shock C_7 produces another shock C_8, well visible on schlieren photographs.

Now we focus on the flow structure in the vicinity of the confluence region between the booster exhaust jet and the external stream. An interpretation of the observed phenomena, sketched in Fig. 9, reveals the following features:

1) Shock C_9 induced by the flare.

2) Shock system, C_{10} and C_{11}, forming in the confluence region between the external flow and the booster exhaust jet. Shock C_{11} is close to the continuation of the compression shock C_1.

3) Slip line Σ_2 dividing the external flow from the jet downstream of the confluence region.

4) The mixing zones (barely visible on the photographs) developing from the separation points along the isobaric boundaries f_3 and f_4.

No perturbation is visible at the separation point at the end of the flare. It indicates that the base pressure is close to the static pressure on the flare. Along Σ_2, a viscous wake develops. Shocks C_9 and C_{11} intersect at point J generating a type IV shock interference according to the terminology introduced by Edney.[17,18] Point J is the origin of a slip line not visible on the photograph.

Surface Flow Visualizations

The model surfaces were coated with an oil film before the run. On photographs taken at the end of the run (see Figs. 10a and 10b), we clearly observe the formation in the skin-friction line pattern of several separation lines on the fuselage and the boosters. These lines are mainly generated by the interaction of the jets with the external flow. The static pressure ratios of the central and lateral jets are equal to 25.7 and 63.5, respectively.

Video recordings of these pictures were also made, permitting an examination of the time evolution of the surface flow. This kind of information is particularly valuable for the construction of the general skin-friction pattern, since it gives the sense of the surface motion. For example, an accumulation of oil and time history of the buildup in the booster-centerbody intersection can be observed at the shoulder of the central base.

Surface flow visualizations will be interpreted in terms of critical points and separation lines, in accordance with Legendre[19] and

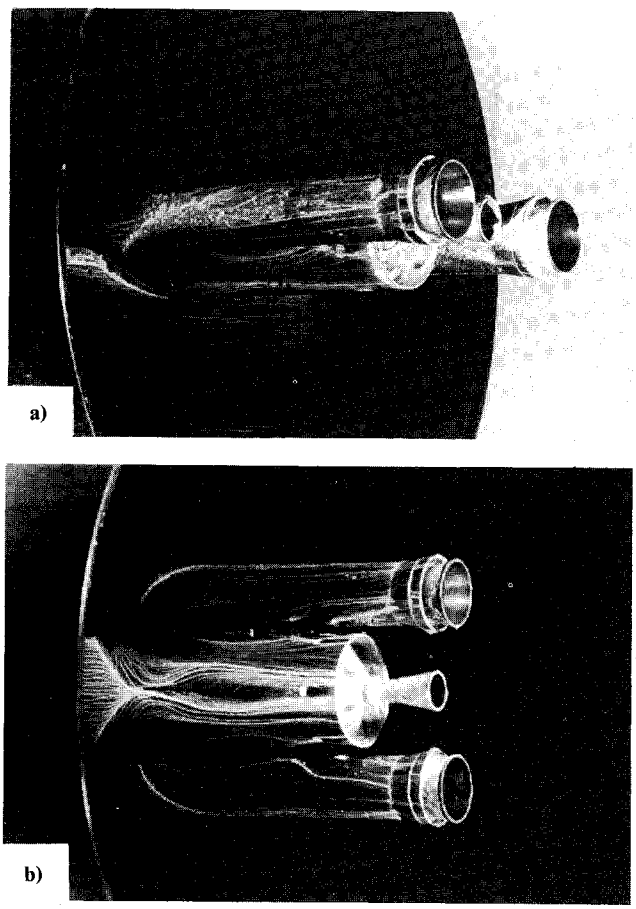

Fig. 10 Surface flow visualization. Nozzle expansion ratio: central engine ($p_j/p_0)_c = 25.7$ and lateral booster engine ($p_j/p_0)_l = 63.5$.

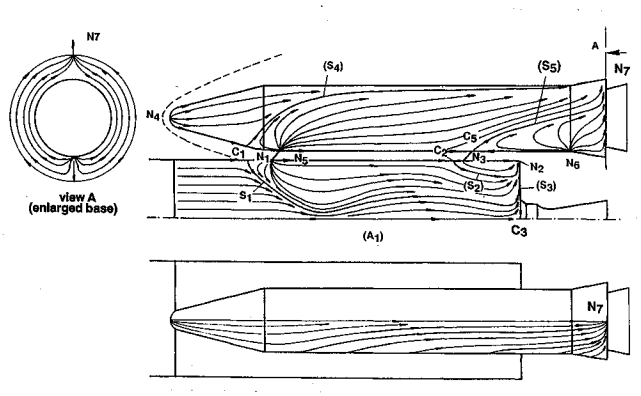

Fig. 11 Interpretation of the surface flow visualization.

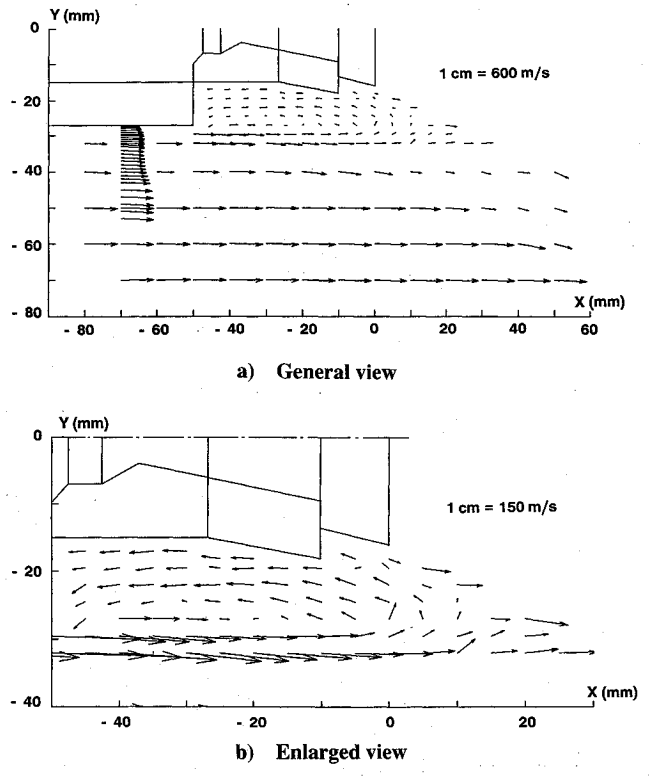

Fig. 12 Mean velocity field in the *OXY* symmetry plane. Nozzle expansion ratio: central engine $(p_j/p_0)_c = 23.2$ and lateral booster engine $(p_j/p_0)_l = 58$.

Lighthill[20] analyses. As we know, three kinds of singular points exist, namely: nodes, focii, and saddle points. Simple topological rules govern the set of nodes, focii, and saddle points that may coexist on a given obstacle. Any separated three-dimensional flow has at least one saddle point, through which two "separators" pass. Such a skin-friction line divides the surface flow pattern into two domains. There are two kinds of "separator" lines: attachment lines and separation lines. These considerations can also be applied to any projection of the velocity vector field on a plane and they are extremely useful to interpret field measurements.

The surface flow pattern observed on the afterbody is represented in Fig. 11. We clearly distinguish the separation line S_1 issued from saddle point C_1 located in the symmetry plane *OXZ* containing the axes of the nozzles (see Fig. 4), upstream of the booster-centerbody joining part. Line S_1 first goes toward the other symmetry plane *OXY* and comes very close to the attachment line A_1. Then, it moves away from A_1 and, near the base, abruptly deflects toward the separation node N_2, practically following the base shoulder. Downstream of saddle point C_1, a first family of streamlines starts from an attachment node N_1 located very near the joining part. Separation line S_1 divides this family from a second family that is formed by the skin-friction lines originating from a nonvisible upstream node type point. A second separation line S_2, issuing from saddle point C_2, separates the previous first family from a third family made of the skin-friction lines originating at node N_3. The three families end at the separation node N_2.

The description of this part of the flow must be completed by the introduction of a separation line S_3 passing through saddle point C_3 and coincident with the base edge. Note that N_2 is at the origin of the streamline family winding around focus F_6 (shown in Fig. 15, derived from LDV results).

The main separation S_1 is certainly provoked by the impact on the centerbody of the booster nose shock wave. The cause of the other separation line S_2 may be either the perturbation originating at the joining strut extremity, or an interaction effect due to jet pluming. These surface visualizations, if correctly interpreted, do not show catastrophic separation zones that would be induced by jet pluming for these nozzle expansion ratios. But it is probable that the size of the separated regions is controlled by the shape of the jets according to a downstream influence that propagates upstream via the separated zones.

Velocity Vector Field Measurements

Exploration of the velocity vector field around the afterbody was the major part of the test program. Measurements with the LDV system have been performed in several planes perpendicular and parallel to the centerbody axis. The ability to rotate the model around this axis allowed a detailed exploration of the velocity field in the space between the central engine and the lateral boosters. In what follows, we will only present results relative to the *OYX* and *OZX* planes of symmetry. These results give a detailed description of the backflow structure in the base region with static pressure ratios equal to 23.2 and 58 for the central and lateral nozzles, respectively.

The velocity field in the symmetry plane *OXY* is shown in Fig. 12a. In this configuration, the axes of the three nozzles are contained in a horizontal plane. This figure shows a detailed profile of the boundary layer on the centerbody upstream of the base. The high value of the boundary-layer thickness, about 20 mm, as also the distorted shape of the profile can be attributed to two reasons:

1) The length of the central sting which is equal to 1.30 m.

2) The location of this profile in a three-dimensional separated zone strongly influenced by booster nose shocks.

Upstream of the centerbody base, the flow outside the boundary layer is nearly uniform. Further downstream, there is a progressive deflection near the model. This deflection, when accompanied by a deceleration of the flow, shows the presence of a compression wave generated by the confluence between the external flow and the jet exhausting from the central nozzle.

The enlargement of the base region shown in Fig. 12b reveals a backflow with a maximum velocity close to 140 m/s. In particular, we note the mixing zone between the dead-air region in contact with the base and the external stream as well as the flow structure in the confluence region.

Measurement points in the recirculation region are not close enough to each other to draw the exact streamlines. However, knowing the vector field, it is possible to give a realistic representation of the streamline pattern in this symmetry plane. As shown in Fig. 13, portions of the streamlines coming from upstream wind around focus F_5 to constitute a recirculating flow or vortex. These streamlines are concentrated between the centerbody and a separation line S_6 ending at a half-saddle point C_6 located near the nozzle exit plane (measurements are not fine enough to precisely define the location of point C_6). Therefore, line S_6 separates streamlines flowing toward the bottom of the centerbody from those carried away along the jet direction. Among these streamlines, those closest to S_6 turn around the recirculation "bubble," thus flowing first toward the base, before being sharply deflected in the downstream direction under the strong entrainment influence of the plume. Hypothetical streamlines, in the jet and backflow regions masked by the booster, are represented by dashed lines for a better understanding of the general flow pattern.

The flowfield measured in the symmetry plane *OXZ* is shown in Fig. 14a. The boundary-layer thickness at the survey location on the booster is approximately equal to 5 mm and its velocity profile is typically turbulent. Here, we note in the upper part of the figure

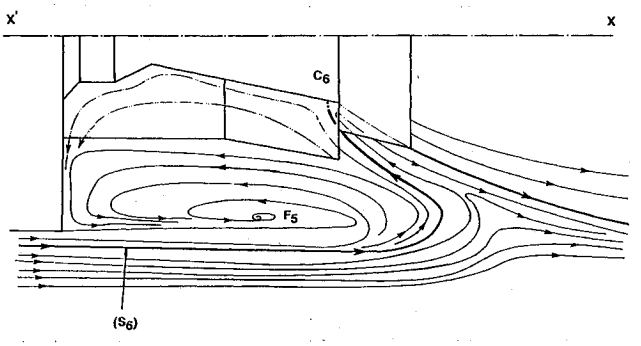

Fig. 13 Mean flow streamlines in the *OXY* symmetry plane.

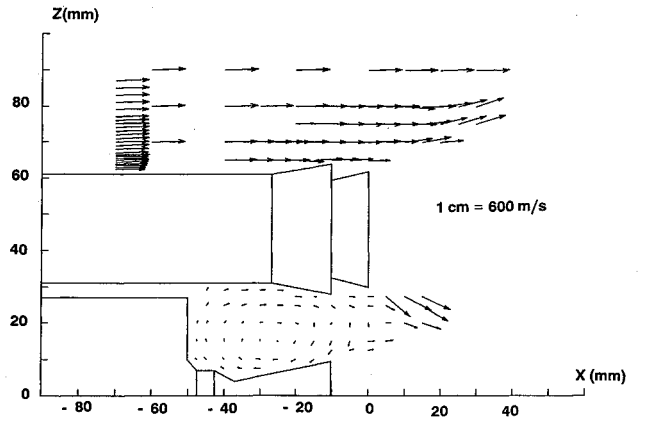

a) General view

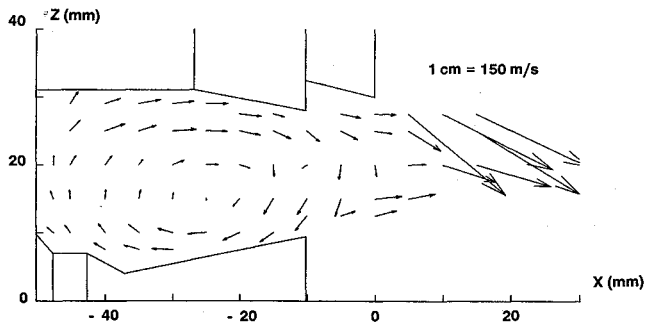

b) Enlarged view

Fig. 14 Mean velocity field in the *OXZ* symmetry plane. Nozzle expansion ratio: central engine $(p_j/p_0)_c = 23.2$ and lateral booster engine $(p_j/p_0)_l = 58$.

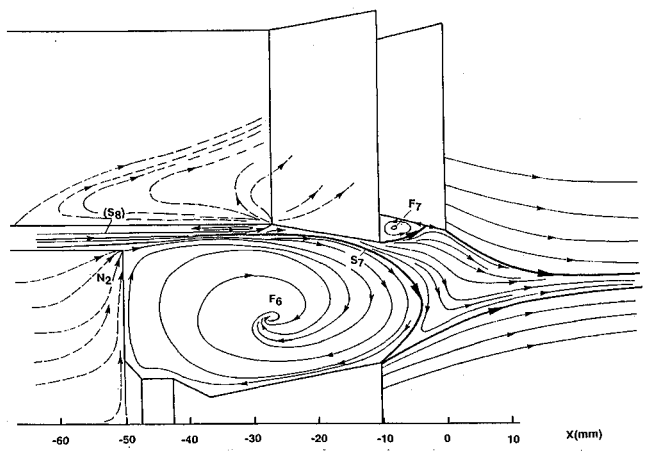

Fig. 15 Mean flow streamlines in the *OXZ* symmetry plane.

the deflection of the velocity vectors due to the presence of the jet exhausting from the booster nozzle. This jet is also visible downstream of the base region near the confluence zone. Over the upstream part of the model, the velocity is uniform and equal to 645 m/s. For a wind-tunnel stagnation temperature of 270 K, this velocity corresponds to a Mach number close to 4.05. The small difference in Mach number, compared to the freestream Mach number of 4.14, is explained by the loss of total pressure through the shock wave produced by the booster nose.

The flow structure in the base region is more clearly shown in the enlarged representation of the field given in Fig. 14b. From this velocity field, it is possible to establish the streamline pattern represented in Fig. 15, which is connected to the skin-friction line pattern of Fig. 11. This pattern shows the existence of a focus F_6 around which wind the streamlines forming the so-called recirculating flow. These lines belong to a family delineated by a separation line S_7 emanating from the central nozzle lip, the origin of S_7 representing the separation node N_2. Therefore, the streamlines passing between the centerbody and S_7 vanish into F_6. As mentioned above, an attachment node—or a stagnation point—exists at the origin of the booster flare, where separation line S_8 terminates. Consequently, the streamlines confined between S_8 and the booster flow backward in the upstream direction. Those contained between S_7 and S_8 go downstream. As shown in Fig. 15, some of the streamlines pass around the recirculating region before being abruptly turned in the downstream direction under the action of the jet entrainment effect. A second recirculation flow, organized around a focus F_7, must exist just behind the booster flare and a separation line ends at a saddle point located on the booster nozzle.

Note that the streamlines sketched in Figs. 13 and 15 are fictitious, since they are associated with a mean flow in the sense of statistical turbulence (Reynolds averaging). In reality, the flow in the base and confluence regions is strongly turbulent, so its instantaneous structure is much more complex than the patterns represented here. However, these mean streamline patterns have the same nature as those resulting from a time-averaged Navier-Stokes calculation. Therefore, they constitute a basis for theoretical/experimental comparisons.

According to Figs. 13 and 15, the streamlines feeding the recirculating zones come from upstream, hence from a cold air region. This is confirmed both by mean field measurements and by application of topological rules. Sketches may create the wrong impression that dead-air regions are filled with cold gas only. In fact, in the case of an actual engine, intense turbulent mass and energy transfer occur across the jet mixing zones and in the confluence region. Consequently, the represented mean flow has strongly varying properties, the recirculating flows being supplied with high enthalpy gaseous species. Therefore, the afterbody surfaces impacted by these hot gases will be submitted to intense heat transfer rates, with an additional risk of a base afterburning if the species are only partially burned.

V. Conclusion

A detailed experimental investigation of the flowfield past a multinozzle afterbody was performed on a 0.01-scale model of the first stage of the ARIANE 5 European launcher. The experimental setup, installed in a blow-down wind tunnel, was constituted by a Mach 4 annular nozzle containing a centerbody holding the model. The three propulsive jets were simulated by high-pressure air at near ambient temperature. The field was analyzed by several means of investigation: surface and stagnation pressure measurements, schlieren photographs, surface flow visualizations, and three-component laser velocimetry.

The surface flow patterns show several separation lines denoting the existence of three-dimensional separation zones. The extension of these separated regions probably depends on jet pluming influence that propagates through the separated zone and the base flow. This phenomenon is confirmed by pressure measurements on afterbody surfaces. Large recirculating flows in base regions were detected by LDV measurements. In particular, strong backflows toward the base cavity of the centerbody were observed.

Probably for the first time, LDV explorations provided precisely defined flow structure and velocity values in such a complex three-dimensional base region. Thus, this work provided detailed knowledge of the nature of the flowfield in the vicinity of the ARIANE 5 launcher afterbody simulating a flight altitude (30 km), where the probability of high heat transfers is the highest. In addition, the results thus obtained can constitute a well-documented test case to validate Navier-Stokes codes.

Acknowledgments

The present study has been performed under contract from the Centre National d'Etudes Spatiales (CNES). Experiments have been carried out in the ONERA R2CH wind tunnel of the Experimental Aerodynamics Branch and the LDV measurements performed by the Laser Velocimetry Group of the same Branch.

References

[1]Kramer, O. G., "Evaluation of Thermal Radiation from the TITAN III Solid Rocket Motor Exhaust Plumes," AIAA Paper 70-842, July 1970.

[2]Greenwood, T. F., Lee, Y. C., Bender, R. L., and Carter, R. E., "Space Shuttle Base Heating," AIAA Paper 83-1544, June 1983.

[3]Délery, J., and Lacau, R. G., "Prediction of Base Flows," *Special Course on Missile Aerodynamics,* AGARD Rept. No. 754, April 1988.

[4]Goethert, B. H., "Base Flow Characteristics of a Missile with Cluster —Rocket Exhausts," IAS Paper 60-89, June 1960.

[5]Musial, N. T., and Ward, J. J., "Base Flow Characteristics for Several Four Clustered Rocket Configurations at Mach Numbers from 2 to 3.5," NASA TN D-1093, Dec. 1961.

[6]Charczenko, N., and Hayes, C., "Jet Effects at Supersonic Speeds on Base and Afterbody Pressures of a Missile Model Having Single and Multiple Jets," NASA TN D-2046, Nov. 1963.

[7]Goethert, B. H., and Matz, R., "Experimental Investigation of Base Flow Characteristics of Four Nozzle Cluster-Rocket Models," AGARDograph No. 87, Vol. 2, 1964.

[8]Korst, H. H., "A Theory for Base Pressure in Two-Dimensional Flow at Supersonic Speeds," *Journal of Applied Mechanics,* Vol. 23, Dec. 1956, pp. 593–600.

[9]Addy, A. L., "Analysis of the Axisymmetric Base Pressure and Base Temperature Problem with Supersonic Interacting Freestream—Nozzle Flows Based on the Flow Model of Korst et al. Part I, II, and III," U.S. Army Missile Command, Rept. RD-TR-69-12, Redstone Arsenal, AL, July 1969.

[10]Reijasse, P., Benay, R., Délery, J., and Lacau, R. G., "Missile and Projectile Base-Flow Prediction by Multi-Component Methods," AIAA Paper 88-4380, Aug. 1988.

[11]Petrie, H. L., and Walker, B. J., "Comparison of Experiment and Computation for a Missile Base Region Flowfield with a Centered Propulsive Jet," AIAA Paper 85-1618, July 1985.

[12]Sahu, J., and Nietubicz, C. J., "Numerical Computation of Base-Flow for a Missile in the Presence of a Centered Jet," AIAA Paper 84-0527, Jan. 1984.

[13]Holcomb, J. E., "Three-Dimensional Navier-Stokes Rocket Plume Calculations," AIAA Paper 89-1886, June 1989.

[14]Reijasse, P., "Analyse Expérimentale de l'écoulement au culot de l'arrière-corps du lanceur ARIANE 5: Etude bibliographique et montage," ONERA RT No. 3/4362AY, Dec. 1986.

[15]Reijasse, P., and Délery, J., "Analyse expérimentale de l'écoulement au culot de l'arrière-corps du lanceur ARIANE 5. Exploitation des résultats," ONERA RF No. 6/4362AY, Nov. 1989.

[16]Boutier, A., D'Humières, C., and Soulevant, D., "Three-Dimensional Laser Velocimetry: A Review," 2nd International Symposium on Application of Laser Anemometry to Fluid Mechanics (Lisbon, Portugal), July 1984; see also ONERA TP No. 1984-43, Aug. 1983.

[17]Edney, B., "Anomalous Heat-Transfer and Pressure Distributions on Blunt Bodies at Hypersonic Speeds in the Presence of an Impinging Shock," Aeronautical Inst. of Sweden, FFA Rept. No. 115, Stockholm, Sweden, Feb. 1968.

[18]Délery, J., "Shock/Shock and Shock Wave/Boundary Layer Interactions in Hypersonic Flows," AGARD Rept. No. 761, *Special Course on Aerothermodynamics of Hypersonic Vehicles,* June 1989.

[19]Legendre, R., "Lignes de courant d'un écoulement permanent. Décollement et séparation," *La Recherche Aérospatiale,* No. 1977-6, Nov.–Dec. 1977, pp. 327–335.

[20]Lighthill, M. J., "Attachment and Separation in Three-Dimensional Flows," *Laminar Boundary Layers,* Sec. II 2–6, Oxford Univ. Press, Oxford, England, UK, 1963, pp. 72–82.